JOURNAL OF AIRCRAFT
Vol. 51, No. 6, November–December 2014

Validating Aircraft Models in the Gap Metric

Andrei Dorobantu,* Gary J. Balas,† and Tryphon T. Georgiou‡
University of Minnesota, Minneapolis, Minnesota 55455

DOI: 10.2514/1.C032580

A framework based on the gap metric is proposed to validate mathematical models of aircraft dynamics using flight data. The approach derives stability margin requirements, and hence is ideally suited to support model-based design and certification of flight control algorithms. This paper shows that the gap metric is an extension of the Theil inequality coefficient: a widely used metric for model validation. The approach is demonstrated on a case study with a small unmanned aircraft.

I. Introduction

RELIABLE flight control algorithms are critical to integrating unmanned aircraft systems (UASs) into the airspace. For many potential UAS applications, the design and certification of these algorithms will rely heavily on mathematical models of the aircraft dynamics. Modern aircraft like the F-35 have already taken advantage of model-based design. At the same time, test pilots on the program attribute some of the costly delays and budget overruns on models that failed to recognize design problems as expected [1]. One of the major lessons learned is that better knowledge of model accuracy is required early in the program to efficiently rely on model-based design. In response to this, the aerospace community must develop more effective tools for model validation.

Model validation refers to assessing the predictive accuracy of a model with respect to experimental data. It is perhaps more accurate to describe the term as seeking to ensure that the data do not actually invalidate a given model. Existing techniques can generally be placed in two categories. In the first, a model perturbation is identified that accounts for the discrepancy between simulation and experiment [2–8]. If the perturbation belongs to an allowable set, the result is deemed not to invalidate the model. This approach mostly relies on linear matrix inequality optimizations and provides rigorous conclusions about model quality. However, it is also limited by computational power and the types of model structures that can be analyzed. A second more commonly used approach [9–11] relies on statistical analysis of the estimated output error between simulation and experiment. Typically blind to model structure, this approach is more broadly applicable than optimization-based methods. However, it also provides less rigorous results and no robustness guarantees.

In the present work, a framework based on the gap metric is proposed as a natural set of techniques to validate aircraft models using flight data. The gap metric, and the closely related normalized coprime fractions, have been previously used within the context of model validation [2,3]. The first contribution of the present work is to interpret the gap metric as a modified generalization of an existing and commonly used statistical validation metric: the Theil inequality coefficient (TIC) [10]. A second contribution is to compute the gap metric using flight-test data and relate the result to well-established robustness margins. Finally, a case study based on flight-test data is presented to underscore the practical relevance of the proposed framework.

Compared to TIC analysis, validation in the gap metric provides analytical rigor when applied to linear time-invariant (LTI) models. It is therefore ideally suited to support model-based design of flight control algorithms, which typically rely on linearized models of the aircraft dynamics. The approach links the validation metric to a controls-centric notion of what constitutes an accurate model. It directly allows a comparison of an identified aircraft model to flight data and the derivation of a set of robustness requirements for closed-loop control. As a result, aerospace engineers may gain confidence earlier in the development process that their control algorithms are safe to be implemented on real aircraft.

II. Theoretical Background

The primary objective of this work is to build engineering perspective on the gap metric in order to make it more accessible for model validation and flight control design. To this end, a key connection is drawn between the gap metric and the TIC. The TIC has been used extensively to validate models for a wide range of aerospace systems, including fixed-wing aircraft, helicopters, and missiles [11–14]. Due to this experience, aerospace engineers feel comfortable with the metric and understand how to apply it to real flight data. In general, the TIC compares time-domain output responses, whereas the gap compares time-domain input and output responses. A suitable adaptation of the TIC to incorporate input responses is given to draw the connection. Subsequently, a transition is made into the frequency domain, which allows the gap metric to be expressed in terms of transfer functions for computational purposes.

For single-input single-output (SISO) systems, the TIC is defined as follows:

$$\mathrm{TIC}(\hat{y}_1, \hat{y}_2) = \frac{\sqrt{\frac{1}{n}\sum_{i=1}^{n} (\hat{y}_{1_i} - \hat{y}_{2_i})^2}}{\sqrt{\frac{1}{n}\sum_{i=1}^{n} (\hat{y}_{1_i})^2} + \sqrt{\frac{1}{n}\sum_{i=1}^{n} (\hat{y}_{2_i})^2}} \tag{1}$$

where $\hat{y}_1$ is a sampled simulation time history, and $\hat{y}_2$ is the corresponding output measurement obtained in flight. For this discrete time formulation, n represents the number of data points. Implicit in this definition is the assumption that the input to the simulation and the input to the aircraft are the same. Equation (2) shows a mathematically equivalent formulation of the TIC in continuous time for the output signals y_1 and y_2:

$$\mathrm{TIC}(y_1, y_2) = \frac{\|y_1 - y_2\|_2}{\|y_1\|_2 + \|y_2\|_2} \tag{2}$$

where

$$\|y\|_2 := \sqrt{\int_{-\infty}^{+\infty} y^2 \, \mathrm{d}t}$$

denotes a 2-norm.

Received 20 August 2013; revision received 26 January 2014; accepted for publication 27 January 2014; published online 29 September 2014.

*Ph.D. Candidate, Department of Aerospace Engineering & Mechanics; dorob002@umn.edu.

†Professor, Department of Aerospace Engineering & Mechanics; balas@umn.edu.

‡Professor, Department of Electrical & Computer Engineering; georgiou@umn.edu.

Model validation using the TIC is very intuitive and easy to understand. The metric ranges from zero to one, where lower values indicate a better model. A value of zero corresponds to a perfect match, and a value of one indicates no correlation. Both transient and steady-state deviations are captured by the numerator, which computes a 2-norm on the output error. This norm measures the squared integral of the error. Finally, the TIC is scaled in the denominator by the individual 2-norms of the outputs being compared.

The TIC was originally proposed as a metric for economic forecasting [10]. In many economic forecasting applications, the input is often poorly defined; hence, only output measurements are used for analysis. Accordingly, the TIC was not defined to take into account input signals. For the analysis of aerospace systems, however, the input is an important quantity. Therefore, a reasonable adaptation of the TIC is

$$\mathrm{TIC}_{\mathrm{modified}}(y_1, y_2, u) = \frac{\left\| \begin{bmatrix} u \\ y_1 \end{bmatrix} - \begin{bmatrix} u \\ y_2 \end{bmatrix} \right\|_2}{\left\| \begin{bmatrix} u \\ y_1 \end{bmatrix} \right\|_2 + \left\| \begin{bmatrix} u \\ y_2 \end{bmatrix} \right\|_2} \tag{3}$$

where u is the input signal applied to the simulation and to the real aircraft. Here, the input has no effect on the numerator and only modifies the denominator scaling. However, this adaptation of the TIC is insightful because, as shown later in this section, it draws a parallel to the gap metric.

A major shortcoming of the TIC, in any formulation, is the lack of rigorous connection to what constitutes a good model. It is difficult to relate a numerical value of this metric to a specific level of model accuracy. Consequently, there is no interpretation of the TIC in terms of stability margin requirements. Engineers only know that, in general, lower TIC values indicate better models. It turns out that a further modification of Eq. (3) leads to a rigorous metric: namely, the gap metric. As a result, model validation gains a connection between model accuracy and closed-loop robustness margins provided by the gap metric.

In the context of feedback control, the gap metric represents a natural notion of the dissimilarity between systems. Closeness in the gap is equivalent to similarity between two systems in an input–output sense. Therefore, the gap metric is suitable for use with experimental flight data. Furthermore, the gap metric quantifies model perturbations that do not destroy feedback stability and taps onto a rigorous foundation of modern robust control with optimization tools and robustness margins. Intuitively, the gap metric differs from the TIC by allowing the inputs (e.g., simulation and experimental inputs) to be different in the analysis. Allowing the inputs to differ is convenient for model validation. For example, consider the case where unmodeled time delays cause a misalignment in the output signals. This type of data discrepancy is commonly found in flight control applications. The resulting TIC would be large, even though the primary dynamics are captured accurately by the model. In practice, engineers address this issue in an ad hoc way by time shifting the signals manually. The gap metric allows the inputs to differ, and be selected accordingly, in order to minimize the overall deviation between the input–output signal pairs. The resulting gap would be small in this example, correctly indicating an accurate model.

To formally define the gap metric, consider two SISO systems P_1 and P_2 with inputs u_1 and u_2 and outputs y_1 and y_2. The gap metric is defined as the maximum of two directed gaps $\vec{\delta}(P_1, P_2)$ and $\vec{\delta}(P_2, P_1)$ [15,16], where

$$\vec{\delta}(P_1, P_2) = \sup_{\|u_1\|_2 \le 1} \inf_{u_2} \frac{\left\| \begin{bmatrix} u_1 \\ y_1 \end{bmatrix} - \begin{bmatrix} u_2 \\ y_2 \end{bmatrix} \right\|_2}{\left\| \begin{bmatrix} u_1 \\ y_1 \end{bmatrix} \right\|_2} \tag{4}$$

Thus, the gap metric is given by:

$$\delta(P_1, P_2) = \max\{\vec{\delta}(P_1, P_2), \vec{\delta}(P_2, P_1)\} \tag{5}$$

The constraint on the supremum in Eq. (4) bounds the 2-norm of u_1, which is a standard condition for maximum–minimum optimizations. Similar to the TIC, the gap metric ranges from zero to one and measures deviations based on 2-norms. Equation (4) shows that the system adaptation of the TIC is a nearly special case of the gap metric, namely, where $u_1 = u_2$ and with a different scale factor in the denominator. Hence, the gap metric can be thought of as a modified generalization of the TIC.

The theory of the gap metric has been advanced by many authors [15–22]. However, in general, it is difficult to compute the gap metric using Eq. (4); moreover, stronger assumptions are needed to enable model validation using flight data. Yet, for P_1 and P_2 being SISO LTI systems with transfer functions $P_1(s)$ and $P_2(s)$, an equivalent formulation exists in the frequency domain [17,19]. Thus, the gap metric can be expressed in both the time and frequency domains, much like system identification techniques used by the aerospace community. System identification is closely related to model validation, and a variety of techniques based in the time and frequency domains have been developed [9,11,12,23]. Model validation using the gap metric is particularly convenient and powerful in the frequency domain, and it aligns with many popular system identification applications [24–27].

A brief introduction to normalized coprime factors follows to introduce the required frequency-domain gap metric theory. Coprime factors are used in control theory to model uncertainty and quantify stability and robustness properties of closed-loop systems [28,29]. Given a transfer function $P_1(s)$, define its numerator and denominator (coprime) polynomials $\tilde{N}_1(s)$ and $\tilde{D}_1(s)$ such that $P_1(s) = \tilde{N}_1(s)/\tilde{D}_1(s)$. The normalized coprime factorization of $P_1(s)$ is

$$P_1(s) = N_1(s)/D_1(s) \tag{6}$$

where the so-called "normalized coprime factors"

$$N_1(s) = \tilde{N}_1(s)/Z_1(s) \quad \text{and} \quad D_1(s) = \tilde{D}_1(s)/Z_1(s) \tag{7}$$

are stable proper transfer functions, instead of polynomials, and satisfy

$$N_1(s)N_1(-s) + D_1(s)D_1(-s) = 1 \tag{8}$$

This also requires $Z_1(s)$ to be stable and satisfy

$$\tilde{N}_1(s)\tilde{N}_1(-s) + \tilde{D}_1(s)\tilde{D}_1(-s) = Z_1(s)Z_1(-s)$$

Normalized coprime factors are key to relating the time-domain gap metric to the frequency domain. Equation (8) will simplify the gap metric later to enable use with flight data.

The gap metric is expressed in the frequency domain as follows:

$$\vec{\delta}(P_1, P_2) = \inf_{Q \in \mathcal{H}_\infty} \|\boldsymbol{G}_1 - \boldsymbol{G}_2 Q\|_\infty \tag{9}$$

which amounts to minimizing the peak gain (i.e., the $\mathcal{H}_\infty$-norm) of a transfer function representing mismatch between the two systems. Here, $\boldsymbol{G}_1(s) = [D_1(s); N_1(s)]$ and $\boldsymbol{G}_2(s) = [D_2(s); N_2(s)]$ are the normalized coprime factors stacked into column vectors, and $Q(s)$ is a scale factor decision variable restricted to be a stable transfer function. The vectors $\boldsymbol{G}_1(s)$ and $\boldsymbol{G}_2(s)$ have interpretations as "graph operators" representing the inputs and outputs of $P_1(s)$ and $P_2(s)$, thus linking the time-domain gap metric to the frequency domain. In fact, $Q(s)$ establishes the correspondence necessary between the inputs to be consistent with the optimization in Eq. (4). For more details on graph operators, see [19,22]. Although the optimization in Eq. (9) is convex and can therefore be solved efficiently, it cannot be used for model validation with flight data in its current form. Note that Eq. (9) requires coprime factorizations, which are not directly

available to engineers. Only time histories and frequency responses (via system identification) can be obtained from flight experiments.

The ν-gap metric is a far-reaching modification to the gap metric that enables more direct computation and connects the analysis to frequency responses [20,22]. This is key for applications to model validation because frequency responses are easily obtained from flight data. Again, the mathematical details on the modification (see [22]) are beyond the scope of this work. Briefly, the ν-gap relaxes the optimization constraint in Eq. (9) from $Q(s) \in \mathcal{H}_\infty$ to allow $Q(s)$ to be an unstable transfer function. However, a new "winding number" condition is needed to counter an unintended side effect on the norm. This condition requires that a term related to the aircraft dynamics (defined subsequently) has equal numbers of unstable poles and zeros. If the condition is not satisfied, then the ν-gap metric defaults to its worst-case value of one. Accordingly, define $\mathcal{S}$ as the set of all transfer functions that have the same number of unstable poles and zeros.

For conventional fixed-wing rigid-body aircraft, it can be assumed that the winding number condition is satisfied. The flight dynamics of these aircraft are easily controlled, and there are no "approximate" unstable pole-zero cancellations. Proximity between unstable poles and zeros relates to the winding number condition and has a detrimental effect on robustness [22]. Formally, the ν-gap is expressed as

$$\delta_\nu(P_1, P_2) = \inf_{Q \in \mathcal{S}} \|\boldsymbol{G}_1 - \boldsymbol{G}_2 Q\|_\infty \tag{10}$$

and there is no distinction between directed formulas.

To explain the connection between the ν-gap and frequency responses, let $\boldsymbol{G}_2^*(s) = \boldsymbol{G}_2(-s)^T$, where $(\cdot)^T$ denotes the transpose. Recall that $\boldsymbol{G}_2(s)$ contains normalized coprime factors, and by Eq. (8), $\boldsymbol{G}_2^*(s)\boldsymbol{G}_2(s) = 1$. Also let $\tilde{\boldsymbol{G}}_2(s) = [N_2(s), -D_2(s)]$, for which $\tilde{\boldsymbol{G}}_2(s)\boldsymbol{G}_2(s) = 0$. Premultiply the term $\boldsymbol{G}_1 - \boldsymbol{G}_2 Q$ in Eq. (10) by $\left[\boldsymbol{G}_2^*; \tilde{\boldsymbol{G}}_2\right]$, which is a unitary matrix, and therefore does not affect the magnitude of the norm:

$$\delta_\nu(P_1, P_2) = \inf_{Q \in \mathcal{S}} \left\| \begin{bmatrix} \boldsymbol{G}_2^*\boldsymbol{G}_1 - \boldsymbol{G}_2^*\boldsymbol{G}_2 Q \\ \tilde{\boldsymbol{G}}_2\boldsymbol{G}_1 - \tilde{\boldsymbol{G}}_2\boldsymbol{G}_2 Q \end{bmatrix} \right\|_\infty \tag{11}$$

$$= \inf_{Q \in \mathcal{S}} \left\| \begin{bmatrix} \boldsymbol{G}_2^*\boldsymbol{G}_1 - Q \\ \tilde{\boldsymbol{G}}_2\boldsymbol{G}_1 \end{bmatrix} \right\|_\infty \tag{12}$$

The key (winding number) assumption on the flight dynamics is that $\boldsymbol{G}_2^*\boldsymbol{G}_1 \in \mathcal{S}$. Therefore, $\delta_\nu(P_1, P_2)$ turns out to be $\|\tilde{\boldsymbol{G}}_2\boldsymbol{G}_1\|_\infty$ since Q can be taken as $Q = \boldsymbol{G}_2^*\boldsymbol{G}_1$. Note that Q is eliminated from the optimization and the solution is an $\mathcal{H}_\infty$-norm. However, the expression still depends on normalized coprime factors. Reference [22] shows how the ν-gap metric can be expressed directly in terms of transfer functions P_1 and P_2 by expanding $\tilde{\boldsymbol{G}}_2\boldsymbol{G}_1$:

$$\begin{aligned} \tilde{\boldsymbol{G}}_2\boldsymbol{G}_1 &= \begin{bmatrix} N_2 - D_2 \end{bmatrix} \begin{bmatrix} D_1 \\ N_1 \end{bmatrix} \\ &= N_2 D_1 - D_2 N_1 = D_2(P_2 - P_1)D_1 \\ &= \left(\frac{D_2 D_2^*}{D_2 D_2^* + N_2 N_2^*}\right)^{1/2} (P_2 - P_1) \left(\frac{D_1 D_1^*}{D_1 D_1^* + N_1 N_1^*}\right)^{1/2} \\ &= (1 + P_2 P_2^*)^{-1/2}(P_2 - P_1)(1 + P_1 P_1^*)^{-1/2} \end{aligned}$$

Hence, the ν-gap metric is computed by evaluating by the following norm:

$$\delta_\nu(P_1, P_2) = \|(1 + P_2 P_2^*)^{-1/2}(P_2 - P_1)(1 + P_1 P_1^*)^{-1/2}\|_\infty \tag{13}$$

Computing the ν-gap metric in this way is very convenient from an engineering perspective. The formula depends only on the transfer functions $P_1(s)$ and $P_2(s)$. Therefore, this approach can be applied to flight data using frequency responses. Discretizing over frequency and plugging $P_1(j\omega)$ and $P_2(j\omega)$ into Eq. (13), the ν-gap metric corresponds to the peak magnitude of the norm over all frequency points.

III. Framework for Model Validation

The ν-gap metric is useful in validating models because it links the validation metric to classical measures of robustness [21,22]. It provides more insight to aerospace engineers than current validation metrics, such as the TIC, with regard to the practical meaning of the computed value. At the same time, it retains a similarity to the TIC via the gap metric and its time-domain interpretation. For model validation, the computed value of the ν-gap metric is related to an uncertainty description that accounts for the difference between the identified aircraft model and flight data. The resulting uncertain model is analyzed using robust control techniques to derive stability margins for control. This relationship between the validation metric and robustness requirements is a major advantage of the ν-gap metric. However, certain assumptions are required on the structure of the uncertainty description.

Consider $P_1(s)$ as the identified aircraft model and $P_2(s)$ as the true aircraft dynamics. Gap theory requires that $P_2(s) \in P_\Delta(s)$. Accordingly, the family of models described by $P_\Delta(s)$ is defined as follows:

$$P_\Delta(s) := \left\{ P_1(s)(1 + \delta_1)/(1 - \delta_2) \right\} \tag{14}$$

where δ_1 and δ_2 are complex numbers representing the uncertainty. The values for δ_i can depend on frequency and be thought of as weighting functions characterizing the uncertainty. This is a type of uncertainty model commonly used in robust control applications. If $|\delta_1| \le \epsilon < 1$ and $|\delta_2| \le \epsilon$, then the ν-gap between $P_1(s)$ and $P_2(s)$ is bounded by $\delta_\nu(P_1(s), P_2(s)) < \epsilon$. Hence, the model validation metric is bounded by the size of the uncertainty.

The model $P_\Delta(s)$, evaluated for all frequencies, forms a disk in the complex plane. Thus, at each frequency, the perturbation required to generate $P_2(s)$ based on $P_1(s)$ is contained in this disk. Stability margins can be guaranteed for a controller operating on $P_2(s)$ that was originally designed based on $P_1(s)$. If the stability margins for the controller are sufficiently large and exceed the worst-case perturbation due to the uncertainty in $P_\Delta(s)$, then the closed-loop controller is guaranteed to stabilize the real aircraft. This has profound implications on model-based flight control design. Controllers designed for an aircraft model, regardless of its accuracy, can be guaranteed to be stable in closed-loop when applied on the real system. As a result, they can be safely implemented and flight-tested earlier in the development program. The relationship between the ν-gap and classical stability margins is given by the following [21]:

$$\text{Gain margin} = 20 \log_{10} \frac{1 + \epsilon}{1 - \epsilon} \tag{15}$$

$$\text{Phase margin} = 2 \arcsin \epsilon \tag{16}$$

$$\text{Disk margin} = \frac{2\epsilon}{1 - \epsilon^2} \tag{17}$$

These margins interpret the validation metric as a robustness requirement for control. For example, $\epsilon = 0.38$ is equivalent to standard stability margins of a 6 dB gain margin and a 45 deg phase margin. If the validation result returns an ϵ value less than 0.38, then a controller with standard robustness margins is guaranteed to be stable on the real aircraft.

Consider a simple example where a nominal aircraft model $P_1(s)$ is given by the following:

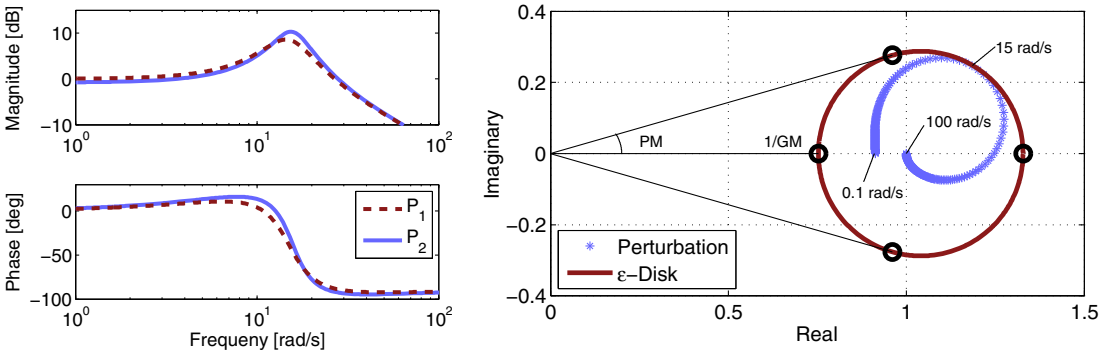

a) Frequency responses b) Perturbations and uncertainty disk

Fig. 1 Comparison of the model $P_1(s)$ and the true aircraft dynamics $P_2(s)$.

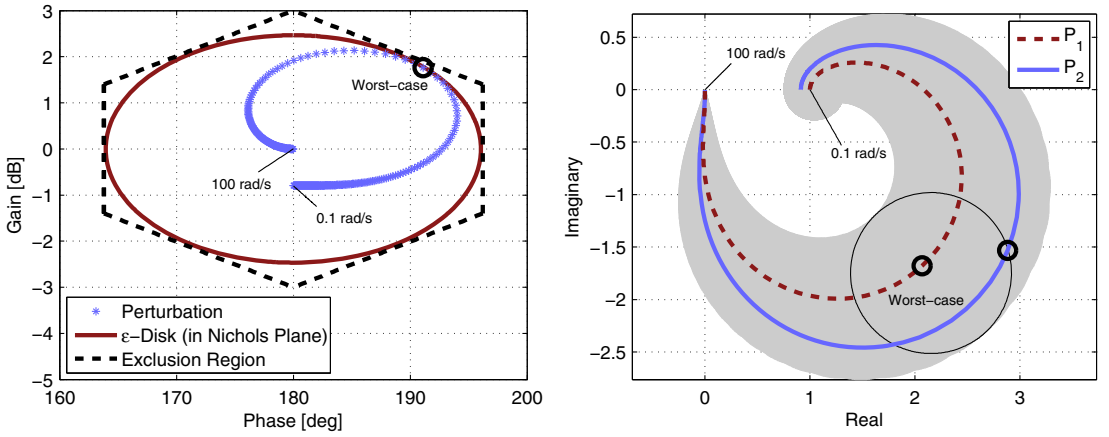

a) Nichols exclusion region b) Robust Nyquist diagram

Fig. 2 Guaranteed robustness margins derived from the gap metric model validation.

$$P_1(s) = \frac{18.75s + 225}{s^2 + 9s + 225} \tag{18}$$

This transfer function is representative of short-period longitudinal dynamics of a small fixed-wing aircraft. Assume that the true aircraft is a perturbation of $P_1(s)$. Uncertainty and errors are expected in the system gain, natural frequency, and damping ratio estimates. For simplicity and without loss of generality, uncertainty in the zero dynamics is neglected. Let the true aircraft dynamics be represented by

$$P_2(s) = \frac{18.75s + 225}{s^2 + 7.22s + 246.5} \tag{19}$$

Given exact knowledge of $P_1(s)$ and $P_2(s)$ in this example, the gap and the ν-gap metrics can be computed directly. Both metrics have the same value of 0.09. It is often the case that values of the gap and the ν-gap are identical. However, this computed value cannot be used directly to infer stability margins. The perturbation between $P_1(s)$ and $P_2(s)$ is not in the assumed coprime factor uncertainty structure required by $P_\Delta(s)$. Therefore, the true aircraft dynamics embodied in $P_2(s)$ must be overbounded by a coprime factor uncertainty model, for which an ϵ value of 0.14 is sufficient. This ensures that the true perturbations are smaller and covered by the coprime factor uncertainty disk associated with $P_\Delta(s)$.

Figure 1, on the right, shows the ϵ disk as a solid circle in the complex plane. Multiplicative perturbations associated with the difference between $P_1(j\omega)$ and $P_2(j\omega)$ [i.e., $P_1(j\omega)/P_2(j\omega)$] are shown for a set of discrete frequency points. The perturbations at 0.1, 15, and 100 rad/s are highlighted. Note that all perturbations are covered by the ϵ disk. Bode plots of $P_1(j\omega)$ and $P_2(j\omega)$ are shown on the left.

Equations (15–17) have geometric interpretations using the ϵ disk. The upper gain margin (GM) is given by the marker on the real axis at 1.33, corresponding to +2.48 dB. Accordingly, the marker on the real axis at 0.75 corresponds to a −2.48 dB gain margin. The phase margin (PM) is given by the angle of the line tangent to the ϵ disk. The markers away from the real axis indicate the tangent points, corresponding to a phase margin of 16.2 deg.

Robustness requirements derived from the model validation analysis can be examined further using Nichols and Nyquist diagrams. Figure 2, on the left, shows the Nichols diagram. Gain and phase variations associated with the ϵ disk form an elliptical region in the Nichols plane. This ellipse is inscribed in a traditional Nichols exclusion region marked by the dashed polygon. The Nichols exclusion region is a useful way to visualize the relationship between the validation analysis and robustness requirements. If a controller satisfies robustness requirements given by the Nichols exclusion region, then the closed-loop system will be stable. Note that the worst-case perturbation near 15 rad/s is on the boundary of the ellipse and inside the Nichols exclusion region.

A robust Nyquist diagram is shown on the right in Fig. 2. The uncertainty associated with the ϵ disk forms a tube around $P_1(s)$ that contains $P_2(s)$. The worst-case perturbation near 15 rad/s is accented with the circular markers. At this frequency, the ϵ disk exactly captures $P_2(s)$. It is important that the shaded region does not cross the critical point at −1 on the real axis, as this would prohibit a stability guarantee for the closed-loop system.

IV. Unmanned Aircraft System Application

The proposed model validation framework is demonstrated for its intended application: evaluating the accuracy of aircraft models with respect to experimental flight data. The data used in this example were obtained with an Ultra Stick 25e aircraft operated by the University of Minnesota [30].[§] The aircraft has a fixed-wing airframe

[§]Data available online at www.uav.aem.umn.edu [retrieved 2014].

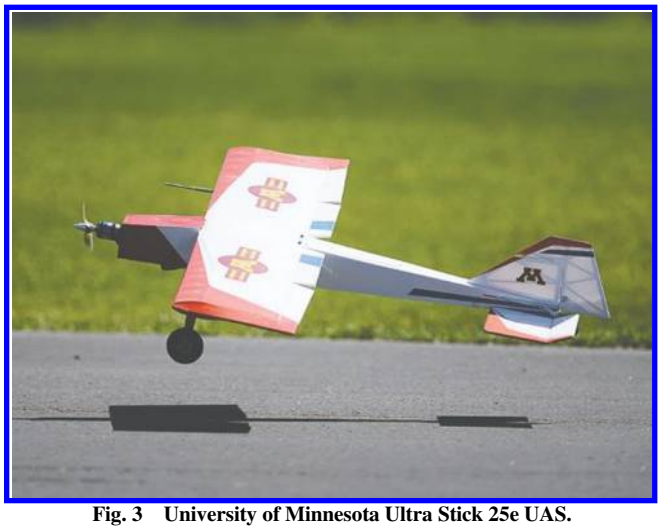

Fig. 3 University of Minnesota Ultra Stick 25e UAS.

with a 2 kg mass and a wingspan of 1.3 m. An inertial measurement unit [31] records angular rates and translational accelerations. Figure 3 shows the aircraft.

A linear model based on constant aerodynamic coefficients was generated using frequency-domain system identification techniques [27]. The trim condition for the experiment was level flight at 19 m/s. Multiple sinusoidal sweep experiments were carried out to obtain data over the primary frequency range of the flight dynamics. Frequency responses were extracted for each input–output data pair, and a parametric state-space model was fitted to the entire dataset. Note that frequency responses used for system identification cannot be reused for model validation. Therefore, two distinct sets of frequency responses were generated.

To be consistent with the previous example, consider $P_1(j\omega)$ as the identified model frequency response to be validated. Let $P_2(j\omega)$ represent the experimental flight data in the form of a frequency response. The model $P_1(j\omega)$ and flight data $P_2(j\omega)$ are shown as Bode plots in Fig. 4. Coherence plots are included below to indicate the quality and accuracy of the frequency responses.

The lightly shaded frequency responses represent the raw data from each individual sinusoidal sweep experiment. In general, data obtained from a single experiment would be sufficient to apply the proposed model validation framework. However, frequency responses based on single experiments often exhibit significant random error. In Fig. 4, for example, the roll rate responses are noisy, particularly at high frequency. Similarly, the yaw rate responses are noisy near the peak of the magnitude. Errors like this contribute directly to more conservative robustness requirements in the validation analysis. This is a consequence of more uncertainty required to overbound the difference between $P_1(j\omega)$ and $P_2(j\omega)$.

The handling of frequency response errors is an engineering decision that depends on the application. In this example, the individual frequency responses are averaged to reduce the effect of random error. The darker solid line in Fig. 4 shows this result. Where the individual roll rate responses are noisy, the average is smooth. A key feature of the proposed validation framework, however, is that it can be applied regardless of data quality. This is particularly beneficial in cases where model accuracy is not crucial and controllers are designed with large stability margins. In these cases, robust stability is guaranteed despite poor data quality. This can significantly reduce the scope and cost of a flight-test campaign.

Figure 5 shows the model validation result for the primary input–output relationships on the aircraft. The lightly shaded markers represent the raw data from individual experiments. Recall that each marker corresponds to the difference between $P_1(j\omega)$ and $P_2(j\omega)$ at a single frequency point. The markers are also related to the lightly shaded frequency responses in Fig. 4. The lightly shaded ϵ disk indicates the main validation result. It shows the amount of uncertainty necessary to account for the perturbations associated with the raw data.

The darker markers in Fig. 5 represent the averaged flight data. These markers also correspond to the darker frequency responses in Fig. 4. The darker ϵ disk indicates the amount of uncertainty necessary to account for the perturbations associated with the averaged data. Note that the darker ϵ disk is significantly smaller than its lighter counterpart. This confirms that averaging the flight data yielded a less conservative uncertainty description. As a result, less stringent robustness requirements have to be satisfied by the controller.

The ϵ disks in Fig. 5 indicate that the elevator-to-pitch-rate model has the highest quality and that the rudder-to–yaw model has the lowest quality. In all three cases, averaging the experimental data reduced the amount of uncertainty necessary to account for the perturbations. Averaging also reduced the random error manifested as scatter, which is indicative of a smoother experimental frequency response. This is particularly noticeable in the roll and yaw rate responses, where the averaged data are qualitatively less scattered

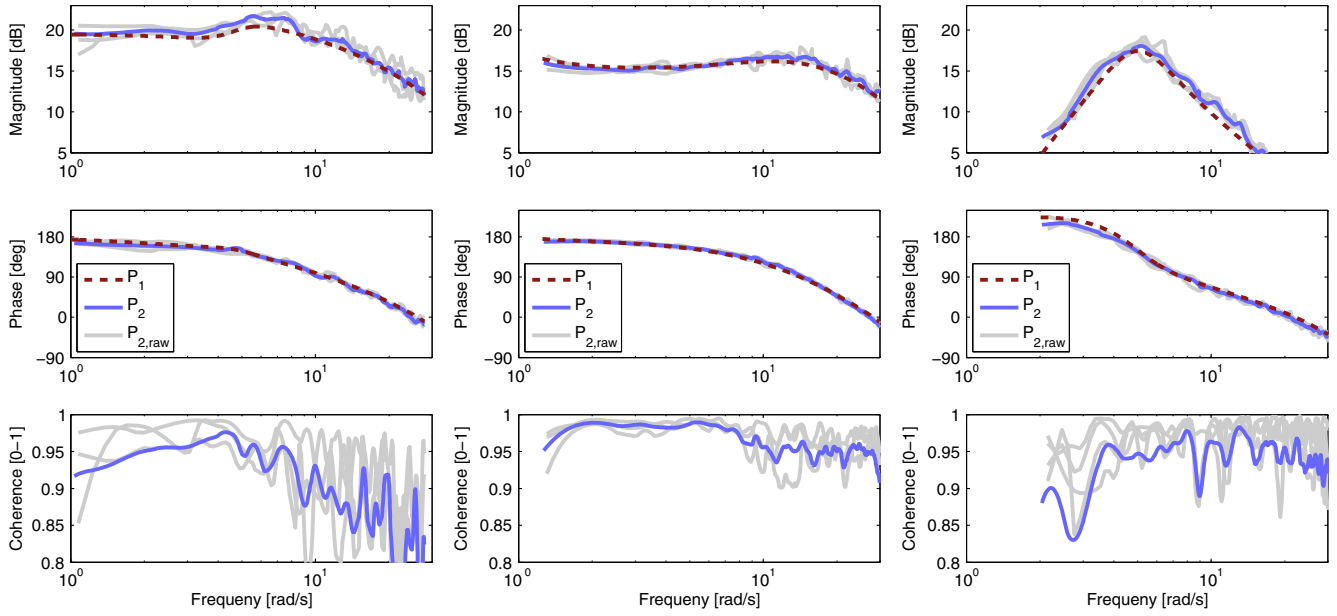

a) Aileron-to-roll rate **b) Elevator-to-pitch rate** **c) Rudder-to-yaw rate**

Fig. 4 Experimental frequency responses compared to the identified linear model.

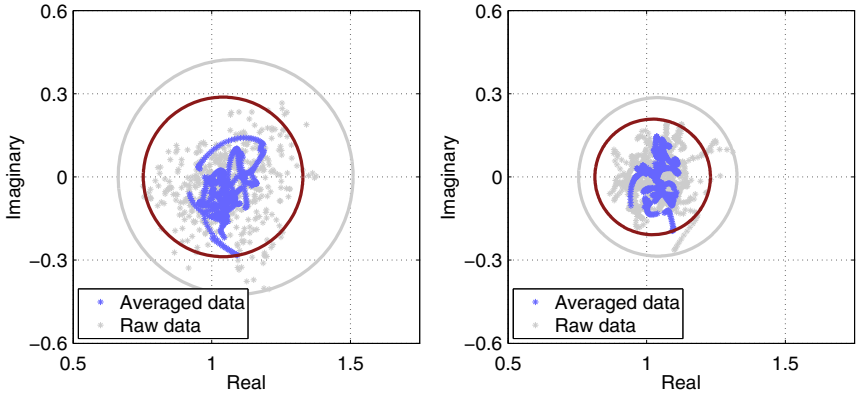

a) Aileron-to-roll rate

b) Elevato-to-pitch rate

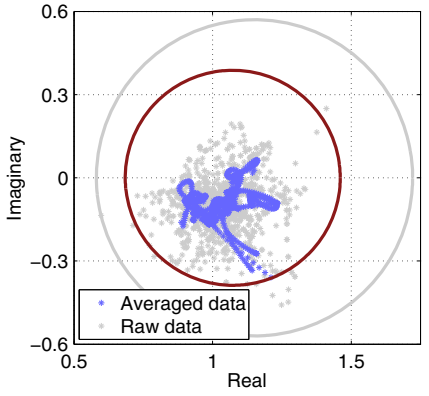

c) Rudder-to-yaw rate

Fig. 5 Perturbations and uncertainty disks relating flight data to the linear model.

and more continuous than the raw data. Table 1 provides a summary of the results.

Table 1 shows how the metric ϵ is related to robustness requirements for closed-loop control. Results are given both for the raw and the averaged data. In comparison to the others, the higher quality of the elevator-to-pitch-rate model is evident from the lower stability margins required for the control system. For the averaged data case, as an example, only about 12 deg of phase margin are required for a controller to be stable. In the rudder-to-yaw-rate model, however, about 21 deg of phase margin are required.

The final step in the validation process is to check that the uncertainty model, which was determined in the frequency domain, translates appropriately into the time domain. A Monte Carlo simulation is executed using input signals recorded from an open-loop doublet flight maneuver. The uncertainty is sampled along the boundary of the ϵ disks and realized as all-pass transfer functions perturbing the nominal model. For this simulation, ϵ disks computed based on the averaged flight data are used. The uncertainty sampling ensures that all possible perturbations in the flight dynamics are represented in the Monte Carlo simulation. For the flight test, a pitch doublet was executed first, followed by a roll doublet, and completed with a yaw doublet. Figure 6 shows the time-domain results by comparing flight data to the Monte Carlo simulations.

Control surface input signals are included in Fig. 6 along with the angular rate measurements. The input signals are shown in degrees but scaled five times in the plot to match the system gain and the order of magnitude of the outputs. The linear aircraft model is represented by the thick dashed line. The flight data are shown by the thick solid line. A lightly shaded tube shows the collection of 500 individual Monte Carlo simulations. This tube corresponds to the family of responses described by the uncertainty model. Note that the main excursions from the tube, which are most significant in the yaw rate response, are caused by unmodeled cross-coupling.

The time-domain simulations provide complementary insight to gap analysis. The flight data match the roll and pitch rate simulations closely. However, the results in Fig. 5 and Table 1 predict that the roll model is significantly less accurate than the pitch model. This discrepancy is caused by erroneous deviation in roll rate frequency response from the identified model, which results in a large gap value (relative to the pitch rate). The deviation is attributed to lower coherence, seen in Fig. 4. Together, gap analysis and the time-domain results provide a clear path forward for the control design. If the computed robustness requirements are acceptable, the model is considered validated and guaranteed stability margins are available. Conversely, if the robustness requirements are not acceptable, the validation analysis points directly to the need for new flight experiments to obtain better quality frequency responses.

The pitch rate model represents the ideal case, where gap analysis correctly predicts a close match in the time-domain simulation.

Table 1 Validation results for raw and averaged flight data

		Roll rate		Pitch rate		Yaw rate	
		Raw	Average	Raw	Average	Raw	Average
Model quality	Gap metric ϵ	0.20	0.14	0.14	0.10	0.27	0.19
Controller requirements	Gain margin, dB	3.58	2.47	2.45	1.80	4.70	3.29
	Phase margin, deg	23.43	16.21	16.10	11.82	30.73	21.29
	Disk margin	0.42	0.28	0.29	0.21	0.57	0.39

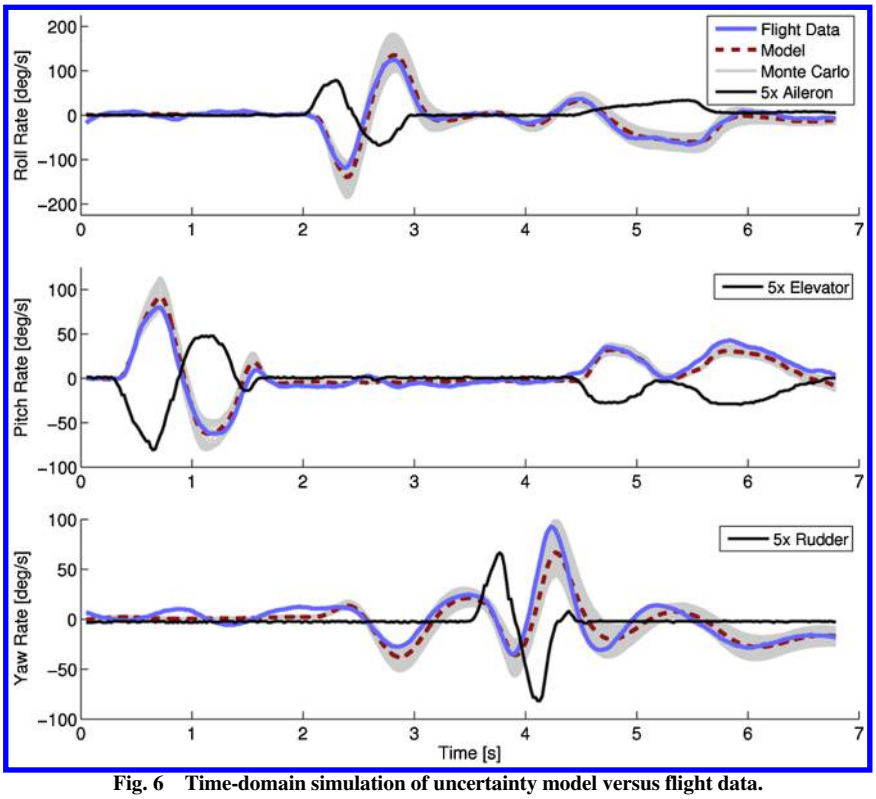

Fig. 6 Time-domain simulation of uncertainty model versus flight data.

These validation results likely provide an acceptable robustness requirement for control design. The yaw rate model represents the final validation case. Here, the computed gap value is large and matches a significant deviation in the time-domain simulation. The deviation indicates that a relatively poor model was identified due to fitting error, and hence that a controller with large robustness margins is needed to stabilize the real closed-loop system. Note, however, that the corresponding uncertainty model successfully accounts for the deviation. In this case, gap analysis shows that the experimental frequency response is accurate, eliminating the need for additional testing. Instead, the underlying modeling and system identification assumptions should be revisited to obtain a better fit.

V. Conclusions

A model validation framework based on the gap metric was described and applied to experimental flight data obtained from a small unmanned aircraft. In the aircraft example, gap values of 0.14, 0.10, and 0.19 were found for the roll, pitch, and yaw rate models, respectively. The proposed framework is powerful because it provides guaranteed robustness requirements for closed-loop control. Accordingly, the computed gap values correspond to 2.47, 1.80, and 3.29 dB gain margins; and 16.21, 11.81, and 21.29 deg phase margin requirements. A major advantage of the proposed framework is that it can be used in model-based flight control design, even if only rough models are available. This can significantly reduce the scope and cost of a certification flight-test campaign. An area of future research is handling multiple-input multiple-output models, allowing cross-coupling relationships to be accounted for directly.

Acknowledgments

This work was partially supported by the NASA grant NNX12AM55A entitled "Analytical Validation Tools for Safety Critical Systems Under Loss-of-Control" monitored by Christine Belcastro; and by the National Science Foundation under grant 0931931 entitled "CPS: Embedded Fault Detection for Low-Cost, Safety-Critical Systems". Any opinions, findings, and conclusions or recommendations expressed are those of the authors and do not necessarily reflect the views of NASA or the National Science Foundation.

References

[1] Hennigan, W. J., and Vartabedian, R., "F-35 Fighter Jet Struggles to Take Off," *Los Angeles Times*, June 2013.

[2] Davis, R. A., "Model Validation for Robust Control," Ph.D. Thesis, Univ. of Cambridge, Cambridge, England, U.K., 1995.

[3] Davis, R., and Glover, K., "An Application of Recent Model Validation Techniques to Flight Test Data," *Proceedings of the European Control Conference: Trends in Control: A European Perspective (ECC'95)*, Vol. 2, Springer–Verlag, New York, 1995, pp. 1249–1254.

[4] Smith, R., and Doyle, J., "Model Validation: A Connection Between Robust Control and Identification," *IEEE Transactions on Automatic Control*, Vol. 37, No. 7, 1992, pp. 942–952. doi:10.1109/9.148346

[5] Poolla, K., Khargonekar, P., Tikku, A., Krause, J., and Nagpal, K., "A Time-Domain Approach to Model Validation," *IEEE Transactions on Automatic Control*, Vol. 39, No. 5, 1994, pp. 951–959. doi:10.1109/9.284871

[6] Smith, R., Dullerud, G., Rangan, S., and Poolla, K., "Model Validation for Dynamically Uncertain Systems," *Mathematical Modeling of Systems*, Vol. 3, No. 1, 1997, pp. 43–58. doi:10.1080/13873959708837048

[7] Rangan, S., and Poolla, K., "Time-Domain Validation for Sample-Data Uncertainty Models," *IEEE Transactions on Automatic Control*, Vol. 41, No. 7, 1996, pp. 980–991. doi:10.1109/9.508901

[8] Dullerud, G., and Smith, R., "Sampled-Data Model Validation: An Algorithm and Experimental Application," *International Journal of Robust and Nonlinear Control*, Vol. 6, Nos. 9–10, 1996, pp. 1065–1078. doi:10.1002/(SICI)1099-1239(199611)6:9/103.0.CO;2-N

[9] Klein, V., and Morelli, E., *Aircraft System Identification: Theory and Practice*, AIAA, Reston, VA, 2006.

[10] Theil, H., *Economic Forecasts and Policy*, North-Holland, Amsterdam, 1970.

[11] Tischler, M., and Remple, R., *Aircraft and Rotorcraft System Identification*, AIAA, Reston, VA, 2006.

[12] Jategaonkar, R., *Flight Vehicle System Identification: A Time Domain Methodology*, AIAA, Reston, VA, 2006.

[13] Mota, S. D. J., and Botez, R. M., "New Helicopter Model Identification Method Based on Flight Test Data," *Aeronautical Journal*, Vol. 115, No. 1167, 2011, p. 295.

[14] Kheir, N., and Holmes, W. M., "On Validating Simulation Models of Missile Systems," *Simulation*, Vol. 30, No. 4, 1978, pp. 117–128. doi:10.1177/003754977803000404

[15] Zames, G., and El-Sakkary, A. K., "Unstable Systems and Feedback: The Gap Metric," *Allerton Conference*, IEEE, Piscataway, NJ, 1980, pp. 380–385.

[16] El-Sakkary, A. K., "The Gap Metric: Robustness of Stabilization of Feedback Systems," *IEEE Transactions on Automatic Control*, Vol. 30, No. 3, 1985, pp. 240–247.
doi:10.1109/TAC.1985.1103926

[17] Georgiou, T. T., "On the Computation of the Gap Metric," *Conference on Decision and Control*, IEEE, 1988, pp. 1360–1361.

[18] Glover, K., and McFarlane, D., "Robust Stabilization of Normalized Coprime Factor Plant Descriptions with H_∞-Bounded Uncertainty," *IEEE Transactions on Automatic Control*, Vol. 34, No. 8, 1989, pp. 821–830.
doi:10.1109/9.29424

[19] Georgiou, T. T., and Smith, M. C., "Optimal Robustness in the Gap Metric," *IEEE Transactions on Automatic Control*, Vol. 35, No. 6, 1990, pp. 673–686.
doi:10.1109/9.53546

[20] Vinnicombe, G., "Frequency Domain Uncertainty and the Graph Topology," *IEEE Transactions on Automatic Control*, Vol. 38, No. 9, 1993, pp. 1371–1383.
doi:10.1109/9.237648

[21] Glover, K., Vinnicombe, G., and Papageorgiou, G., "Guaranteed Multi-Loop Stability Margins and the Gap Metric," *Conference on Decision and Control*, IEEE, 2000, pp. 4084–4085.

[22] Vinnicombe, G., *Uncertainty and Feedback: H_∞ Loop-Shaping and the ν-Gap Metric*, World Scientific, Hackensack, NJ, 2001.

[23] Ljung, L., *System Identification: Theory for the User*, 2nd ed., Prentice–Hall, Upper Saddle River, NJ, 1999.

[24] Morelli, E., "Low-Order Equivalent System Identification for the Tu-144LL Supersonic Transport Aircraft," *Journal of Guidance, Control, and Dynamics*, Vol. 26, No. 2, 2003, pp. 354–362.
doi:10.2514/2.5053

[25] Mettler, B., Tischler, M., and Kanade, T., "System Identification of a Small-Scale Unmanned Rotorcraft for Flight Control Design," *Journal of the American Helicopter Society*, Vol. 47, No. 1, 2002, pp. 50–63.
doi:10.4050/JAHS.47.50

[26] Theodore, C., Tischler, M., and Colbourne, J., "Rapid Frequency-Domain Modeling Methods for Unmanned Aerial Vehicle Flight Control Applications," *Journal of Aircraft*, Vol. 41, No. 4, 2004, pp. 735–743.
doi:10.2514/1.4671

[27] Dorobantu, A., Murch, A., Mettler, B., and Balas, G., "System Identification for a Small, Low-Cost, Unmanned Aircraft," *Journal of Aircraft*, Vol. 50, No. 4, 2013, pp. 1117–1130.

[28] Vidyasagar, M., "Control System Synthesis: A Factorization Approach," The MIT Press, Cambridge, MA, 1985, p. 82.

[29] Doyle, J. C., Francis, B. A., and Tennenbaum, A. R., *Feedback Control Theory*, Dover, New York, 2009, pp. 59–63.

[30] Dorobantu, A., Johnson, W., Lie, F. A., Taylor, B., Murch, A., Paw, Y. C., Gebre-Egziabher, D., and Balas, G., "An Airborne Experimental Test Platform: From Theory to Flight," *American Control Conference*, IEEE, Piscataway, NJ, 2013.

[31] "ADIS16405 Triaxial Inertial Sensor with Magnetometer," Analog Devices TR, Norwood, MA, 2009.